

Optical Engineering

SPIDigitalLibrary.org/oe

Novel diffractive optical element: binary photon sieve

Changlun Hou

Novel diffractive optical element: binary photon sieve

Changlun Hou
 Zhejiang University
 State Key Laboratory of Modern Optical
 Instrumentation
 Hangzhou 310027, China
 E-mail: hou_cl@hotmail.com

Abstract. In this paper, we developed a novel photon sieve consisting of a large number of precisely positioned holes distributed according to an underlying Fresnel zone plate (FZP) geometry, while the holes at transparent and opaque circular rings of the FZP have a π phase shift. Compared to a conventional photon sieve which we call an amplitude-photon sieve (PS), the binary photon sieve has a transmission two times more amplitude-PS and a diffractive efficiency approximately four times than amplitude-PS. A 70-mm diameter, $f/10$ binary photon sieve has been fabricated for operation at visible light. Details of design, fabrication, and performance of the binary photon sieve are presented. © 2011 Society of Photo-Optical Instrumentation Engineers (SPIE). [DOI: 10.1117/1.3589294]

Subject terms: photon sieve; diffractive optics; binary optics; micro-optics.

Paper 101035RR received Dec. 7, 2010; revised manuscript received Mar. 28, 2011; accepted for publication Apr. 14, 2011; published online Jun. 6, 2011.

1 Introduction

The photon sieve (PS) is a diffractive element which is derived from a traditional Fresnel zone plate (FZP) and consists of millions of pinholes distributed on transparent circular rings of FZP. Compared with FZP, a large number of holes distributed appropriately over the Fresnel zones make it possible to focus light to a spot size smaller and the higher order of diffraction and secondary maxima can be suppressed significantly. In addition, photon sieve provides the advantage that the size of the focused spot is not limited by the width of the smallest zone. As in the case of traditional FZP, the spatial resolution that can be achieved is of the order of the width of the outermost zone and is therefore limited by the smallest structure that can be fabricated by lithography. The size of the holes can be increased beyond the underlying zone width to permit the construction of a large optic with holes of a reasonable size at the outermost zones within the aperture.¹ The increase in hole diameters greatly reduces the design constraints on fabricating such a device. It is especially important when the width of the zone approaches the lithographic limits.

These characters of the photon sieve show that it has a promising future in high resolution imaging and super narrow width lithography areas. Kipp and his colleagues presented the concept of the photon sieve.¹ They use a pinhole distributed on the Fresnel zone to focus a soft x-ray onto a spot which was smaller than the width of the outermost zone of the Fresnel zone. Menon et al. used a photon sieve in their lithography system as the focus lens. The numerical aperture (NA) of their photon sieve can reach 0.9 and the width of the exposure line can reach 244 nm at 400-nm wavelength.^{2,3} Andersen and his colleagues fabricated a 1-m focal length, 0.1-m diameter photon sieve over a significant bandwidth and had a moderate field of view. They pointed out that PS offers an appealing solution for the construction of next-generation, ultralarge space telescope primaries.⁴⁻⁶ They also said that a flat element can be simply packaged and deployed without the problems associated with creating a diffraction-limited, three-dimensional mirror surface and the photon sieve has no connected regions which permit

the fabrication of a single surface without any supporting struts required. Recently, by combining the concepts of the Fractal zone plate (FraZP) and the photon sieve, the fractal photon sieve (FraPS)⁷⁻⁹ has been developed which not only has similar unique properties as FraZPs but also significantly suppress the high order diffractions.

In the case of amplitude photon sieves, only the pinholes distributed on corresponding transparent circular rings of FZP are transparent, so the focusing efficiency of such a photon sieve is lower than the FZP with the same diameter and focal length. It is significant to improve the focusing efficiency of the photon sieve especially for its use on a high resolution system such as a lithography system and a telescope system. In order to improve efficiency based on photon sieve and binary optics element, we developed a new type of photon sieve which we call binary photon sieve. In the binary photon sieve, millions of holes are distributed on corresponding transparent and opaque circular rings of Fresnel zone-plates, while holes in alternate zones have a π phase shift. By appropriately placing the holes in the transparent and opaque zones, the zero-order diffraction efficiency will be significantly reduced, and consequently, the focusing efficiency will be enhanced.

2 Theory

Figure 1 shows the amplitude-PS and binary photon sieve. On the amplitude-PS, holes are distributed on transparent circular zones, while on the binary photon sieve, holes are distributed not only on transparent circular zones, but also on opaque circular zones. The holes at transparent circular zones and opaque circular zones have a π phase shift.

Cao and Jahns have built a model based on the far-field formula of individual pinholes and the linear superposition principle which is applicable to arbitrary paraxial illumination with arbitrary complex amplitude distribution at the photon sieve plane.^{10,11} Assume a binary photon sieve, which consists of a great number of pinholes whose locations and radii are properly chosen, is located at the xy plane. The desired focal point is located at the point ($X = 0, Y = 0$), the phase shift is between transparent and opaque zones is π , and the distance between the xy plane and the XY plane is q . Because the change of the field inside the pinhole is very

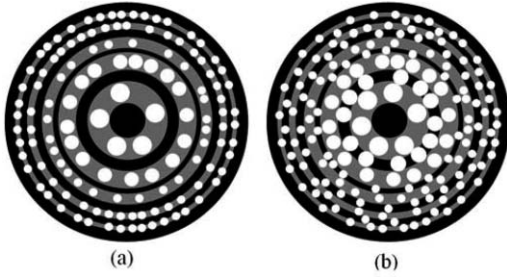


Fig. 1 (a) Schematic of amplitude-PS and (b) binary photon sieve.

small, the complex amplitude distribution inside the pinhole can be expressed as the local plane wave. Assume the local plane wave is the normal illumination. We denote by $A(x, y)\exp[jkL(x, y)]$ the complex amplitude distribution of the paraxial illumination beam at the photon sieve plane, where $k = 2\pi/\lambda$ is the wave number, λ is the wavelength, j is the imaginary unit, $L(x, y)$ is the eikonal, and $A(x, y)$ is the real amplitude. From the Fresnel diffraction integral formula, the corresponding diffracted field $U_n(X, Y)$ at transparent circular zones can be expressed as:

$$U_n(X, Y) = \frac{1}{\lambda q} \int \int_{-\infty}^{\infty} A(x, y) \exp[jkL(x, y)] \times \exp\left[jk \frac{(X-x)^2 + (Y-y)^2}{2q}\right] dx dy. \quad (1)$$

The corresponding diffracted field $U_m(X, Y)$ at opaque circular zones can be expressed as:

$$U_m(X, Y) = \frac{1}{\lambda q} \int \int_{-\infty}^{\infty} A(x, y) \exp[jkL(x, y)] \exp(j\pi) \times \exp\left[jk \frac{(X-x)^2 + (Y-y)^2}{2q}\right] dx dy. \quad (2)$$

In Eqs. (1) and (2), we have ignored the common factor $-j \exp(jkq)$ for simplicity. According to the linear superposition principle, the total diffracted field $U(X, Y)$ at the focal plane is the sum of those individual diffracted fields from different pinholes, as the following equation shows:

$$U(X, Y) = \sum_n U_n(X, Y) + \sum_m U_m(X, Y). \quad (3)$$

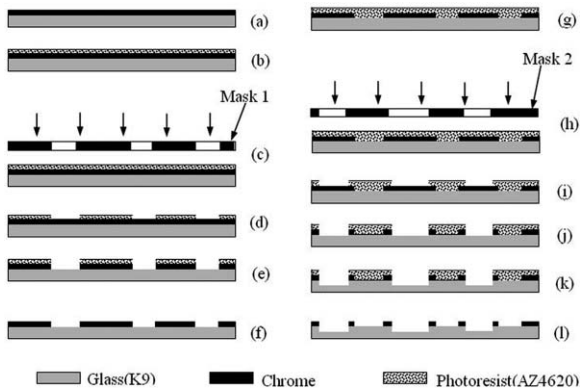


Fig. 2 Fabrication process of binary photon sieve.

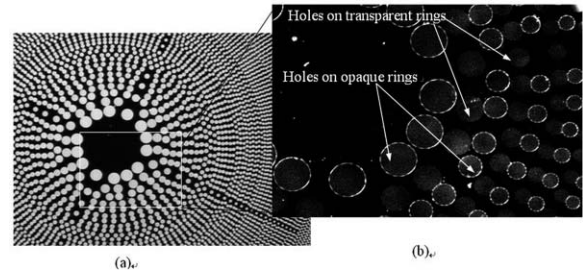


Fig. 3 Photograph of the fabricated binary photon sieve. (a) Zoom 30×, (b) zoom 100×.

Assume the n 'th pinhole, whose central location and radius are denoted by $(x = x_n, y = y_n)$ and a_n , respectively. Equations (1) and (2) can be derived as follows:^{10,11}

$$U_n(X, Y) = 2N_f A_n \exp\left[jk \left(L_n + \frac{R'^2}{2q}\right)\right] \text{Jinc}\left(\frac{ka_n}{q} \cdot \rho\right), \quad (4)$$

where $R' = \sqrt{(X - x_n)^2 + (Y - y_n)^2}$,

$$\rho = \sqrt{(X - x_n - q(\partial L/\partial x)|_{x_n, y_n})^2 + (Y - y_n - q(\partial L/\partial y)|_{x_n, y_n})^2},$$

$L_n = L(x_n, y_n)$, $\text{Jinc}(t) = J_n(t)/t$, $J_n(t)$ is the n 'th-order Bessel function, and $N_f = \pi a_n^2/(\lambda q)$ is the Fresnel number.

The crucial idea of the photon sieve is that all those individual diffracted fields from different holes have the same phase value or have a phase difference of $2m\pi$ at the desired focal point $(X = 0, Y = 0)$. Therefore the selection condition of the pinholes can be briefly stated as follows:

$$k \left(L_n + \frac{r_n^2}{2q}\right) = 2m\pi, \quad \text{Jinc}\left(\frac{ka_n}{q} R_n\right) > 0, \quad (5)$$

$$k \left(L_n + \frac{r_n^2}{2q}\right) = (2m + 1)\pi, \quad \text{Jinc}\left(\frac{ka_n}{q} R_n\right) < 0, \quad (6)$$

where $r_n^2 = x_n^2 + y_n^2$,

$$R_n = \sqrt{(x_n + q(\partial L/\partial x)|_{x_n, y_n})^2 + (y_n + q(\partial L/\partial y)|_{x_n, y_n})^2}.$$

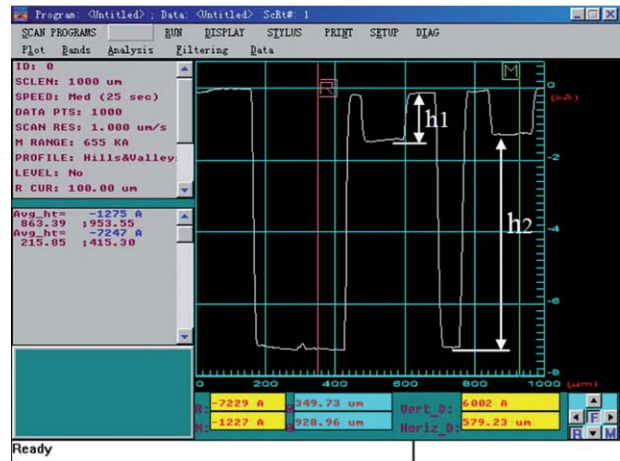


Fig. 4 Step height tested by profiler (h1 is the thickness of the chrome layer and h2 is the step height of the adjacent pinholes).

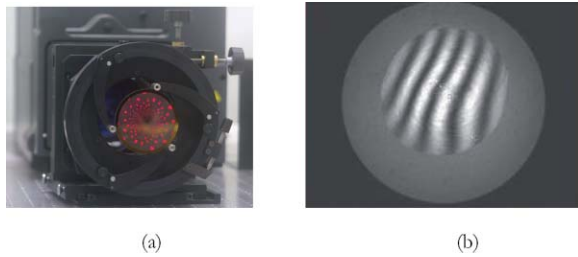


Fig. 5 (a) Photograph of photon sieve illuminated from the rear. (b) Interferogram of the photon sieve.

The above derivation is based on paraxial Fresnel diffraction integral. The 4th order and higher order phase items in spherical phase factors were neglected. This method is fit for a low NA photon sieve; while for a high NA photon sieve, the derivation should be based on a nonparaxial far field model. Specially when the scales of pinhole is close to or even smaller than the diffracted wavelength, a rigorous vector diffraction model such as rigorous coupled wave (RCW) and modal approach should be used.

3 Experimental Results and Discussion

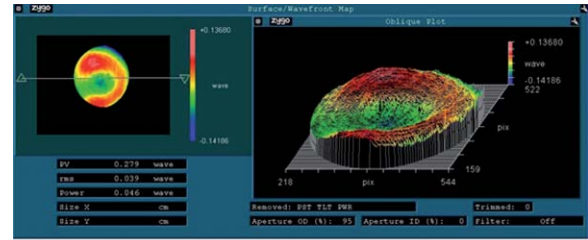
We designed a 70-mm diameter, $f/10$ binary photon sieve. By theoretical analysis, the diameter of the pinholes from the center to the edge ranged from 279.4 to 3.5 μm . Two 4 in. masks were designed to fabricate the binary photon sieve. On mask 1, there are a large amount of pinholes distributed on corresponding transparent circular zones appropriately. On mask 2, there are a large amount of pinholes distributed on corresponding opaque circular zones appropriately. As shown in Fig. 2(a), a glass (K9) plate coated with a 140-nm thick chrome layer was used as a substrate. First, by lithography and wet etching, the figures on mask 1 were replicated on the substrate [as shown in Figs. 2(b)–2(f)]. Cerium ammonia nitrate $[\text{Ce}(\text{NH}_4)_2(\text{NO}_3)_6]$ solution was used to etching chrome layer [as shown in Fig. 2(e)]. Secondly, the same process was done on the substrate with mask 2 [as shown in Figs. 2(g)–2(j)]. At the last step, by the reaction ion beam etching process (RIBE) [as shown in Fig. 3(k)], a step will appear between the holes replicated from mask 1 and mask 2. The step height was decided by the designed wavelength and the refractive index of the substrate material.

All the lithography processes were performed on a 70-cm glass substrate plate, spin coated with 800 nm of AZ4620 (spun at 2500 rpm and baked on a hot plate at 90 °C for 30 min).

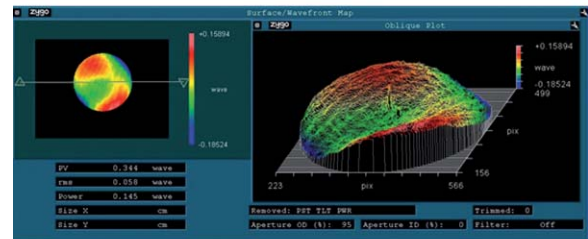
Figures 3(a) and 3(b) show the photographs taken by a stereo microscope of the fabricated binary photon sieve. In

Table 1 Experiment data.

Focus element	Measured intensity	Diffraction efficiency
Lens	1.32 mW	100%
Amplitude-PS	38.82 μW	2.94%
Binary-PS	157.14 μW	11.90%



(a)



(b)

Fig. 6 Wavefront measured by zygo interferometer. (a) Wavefront of amplitude photon sieve, (b) wavefront of binary photon sieve.

Fig. 3(b), the circles with white margin are the pinholes with an etched depth by the RIBE device.

Figure 4 shows the step height of the pinholes at adjacent circular zones tested on a profiler (VEECO DEKTAK 3). The fabricated step height of the pinholes at adjacent circular zones is 600.2 nm and the thickness of the chrome layer is about 140 nm.

The refractive index of the substrate material is 1.515 at wavelength 650 nm. In order to get a π phase shift at adjacent zones, the depth of the step can be calculated as:

$$h = \frac{\lambda}{2 \times (n - 1)} = \frac{650}{2 \times (1.515 - 1)} = 631 \text{ nm}, \quad (7)$$

$$h_{\text{Error}} = \frac{631 - 600.2}{631} = 4.88\%. \quad (8)$$

Because of the instability of the RIBE process caused by the reaction gas during the etching process, there is an error between the real depth and the theoretical depth. As shown in Eq. (8), the relative error is 4.88%. The fabrication error will cause the diffraction efficiency to deduce and bring some background scatter light.

From the distribution of the transparent area, a zone plate has a transmission of 50%, whereas an amplitude photon sieve transmits only 15% to 25% of the incident light.¹ A binary photon sieve can transmit double of the conventional photon sieve. In order to measure the diffractive efficiency of a binary photon sieve and an amplitude photon sieve, a

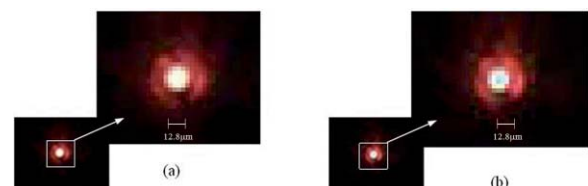


Fig. 7 Images at the focal spot [(a) focal spot of binary photon sieve, (b) focal spot of amplitude photon sieve].

collimated laser beam was illuminated on the binary photon sieve and amplitude photon sieve, respectively, at the focal plane a corresponding focal spot can be observed.

Equation (9) was used to calculate the diffractive efficiency by light intensity at the focal point and the incident intensity of the light:

$$\eta_{\text{diff}} = \frac{I_{\text{Focus}}}{I_{\text{Incident}}} \times 100\%, \quad (9)$$

where η_{diff} is diffractive efficiency, I_{Focus} is the light intensity at the focal point, and I_{Incident} is the intensity of the light illuminating on the photon sieve.

From the experiment data (in Table 1), we can calculate that the diffractive efficiency of the amplitude photon sieve is 2.94% while the diffractive efficiency of the binary photon sieve is 11.90%. The binary photon sieve has a diffractive efficiency about 4 times that of the amplitude photon sieve.

Figure 5 shows the measurement photograph of the binary photon sieve on our zygo interferometer. Figures 6(a) and 6(b) show the transmission wavefront of the amplitude photon sieve and the binary photon sieve tested by the zygo interferometer. The tested PV and rms values of the amplitude photon sieve are 0.279 and 0.039 λ and the tested PV and rms values of the binary photon sieve are 0.344 and 0.058 λ .

Figures 7(a) and 7(b) show the focal spot of the amplitude and binary photon sieves. The model of the CMOS camera is MV-300UC with a pixel array of 2048 \times 1536. The size of each pixel is 3.2 \times 3.2 μm . In the focal spot image of the amplitude photon sieve, the diameter of the focal spot is 5 pixels, and in the focal spot image of binary photon sieve, the diameter of the focal spot is appreciably more than 5 pixels.

4 Conclusion

In summary, we developed a new type of photon sieve which can be regarded as a quasiphase-type photon sieve. The design and fabrication process of the binary photon sieve was introduced. A 70-mm diameter, $f/10$ binary photon sieve was fabricated. From the measured results of transmitted wavefront and focal spot of binary photon sieve and amplitude photon sieve, we can conclude that the binary photon sieve has the same imaging and focus property with a amplitude photon sieve while the binary photon sieve demonstrated a much higher diffractive efficiency (about 4 times) than amplitude-type counterparts. They can be used in high

resolution imaging and super narrow width lithography areas. For example, binary photon sieves have the potential to be primary elements in large space telescopes as they can be constructed from flat membranes. For the diffractive element suffered from large amounts of dispersion, how to compensate for the dispersion will be a key problem in the telescope design.

Acknowledgments

This research was supported by the National Science Foundation (Grant No. 60908025). The authors would like to thank Dr. Xu Jianfeng for the help on the RIBE fabrication process.

References

1. L. Kipp, M. Skibowski, R. L. Johnson, R. Berndt, R. Adelung, S. Harm, and R. Seemann, "Sharper images by focusing soft x-rays with photon sieves," *Nature (London)* **414**, 184–188 (2001).
2. R. Menon, D. Gil, G. Barbastathis, and H. I. Smith, "Photon-sieve lithography," *J. Opt. Soc. Am.* **22**(2), 342–345 (2005).
3. D. Gil, R. Menon, and H. I. Smith, "The case for diffractive optics in maskless lithography," *J. Vac. Sci. Technol. B* **21**(6), 2810–2814, (2003).
4. G. Andersen, "Large optical photon sieve," *Opt. Lett.* **30**(22), 2976–2978 (2005).
5. G. Andersen, "Photon sieve null corrector," *Proc. SPIE* **6273**, 62730K1 (2006).
6. G. Andersen and D. Tullson, "Photon sieve telescope," *Proc. SPIE* **6265**, 626523 (2006).
7. F. Giménez, J. A. Monsoriu, W. D. Furlan, and A. Pons, "Fractal photon sieve," *Opt. Express* **14**(25), 11958–11963 (2006).
8. F. Gimenez, W. D. Furlan, and J. A. Monsoriu, "Lacunar fractal photon sieves," *Opt. Comm.* **277**, 1–4 (2007).
9. Y. J. Liu, H. T. Dai, X. W. Sun, and T. J. Huang, "Electrically switchable phase-type fractal zone plate and fractal photon sieves," *Opt. Express* **17**(15), 12418–12423 (2009).
10. Q. Cao and J. Jahns, "Focusing analysis of the pinhole photon sieve: individual far-field model," *J. Opt. Soc. Am. A* **19**(20), 2387–2393, (2002).
11. Q. Cao, "Diffractive nano-focusing and nano-imaging," *Proc. SPIE* **6342**, 634219 (2006).



Changlun Hou is a research member in the Department of Optical Engineering and State Key Laboratory of Modern Optical Instrumentation at Zhejiang University where his work focused on optical measurement technology and micro-optics sensor. He received a PhD degree in optical engineering from Zhejiang University in 2005 in China.